Warming and Weakening of the Abyssal Flow through Samoan Passage

GUNNAR VOET AND MATTHEW H. ALFORD

Scripps Institution of Oceanography, University of California, San Diego, La Jolla, California

JAMES B. GIRTON

Applied Physics Laboratory, University of Washington, Seattle, Washington

GLENN S. CARTER

University of Hawai'i at Mānoa, Honolulu, Hawaii

JOHN B. MICKETT

Applied Physics Laboratory, University of Washington, Seattle, Washington

JODY M. KLYMAK

University of Victoria, Victoria, British Columbia, Canada

(Manuscript received 15 March 2016, in final form 16 May 2016)

ABSTRACT

The abyssal flow of water through the Samoan Passage accounts for the majority of the bottom water renewal in the North Pacific, thereby making it an important element of the meridional overturning circulation. Here the authors report recent measurements of the flow of dense waters of Antarctic and North Atlantic origin through the Samoan Passage. A 15-month long moored time series of velocity and temperature of the abyssal flow was recorded between 2012 and 2013. This allows for an update of the only prior volume transport time series from the Samoan Passage from WOCE moored measurements between 1992 and 1994. While highly variable on multiple time scales, the overall pattern of the abyssal flow through the Samoan Passage was remarkably steady. The time-mean northward volume transport of about 5.4 Sv (1 Sv $\equiv$ $10^6\,m^3\,s^{-1}$) in 2012/13 was reduced compared to 6.0 Sv measured between 1992 and 1994. This volume transport reduction is significant within 68% confidence limits ($\pm$0.4 Sv) but not at 95% confidence limits ($\pm$0.6 Sv). In agreement with recent studies of the abyssal Pacific, the bottom flow through the Samoan Passage warmed significantly on average by 1×10^{-3}°C yr^{-1} over the past two decades, as observed both in moored and shipboard hydrographic observations. While the warming reflects the recently observed increasing role of the deep oceans for heat uptake, decreasing flow through Samoan Passage may indicate a future weakening of this trend for the abyssal North Pacific.

1. Introduction

The meridional overturning circulation (MOC) is a key element of the global climate system as vast amounts of heat, carbon dioxide, and other tracers are redistributed meridionally and in the vertical. On the order of 30 Sv (1 Sv $\equiv$ $10^6\,m^3\,s^{-1}$) of dense deep and bottom waters are formed in polar regions and feed the lower limb of the MOC (e.g., Lumpkin and Speer 2007). As there is virtually no deep water formation in the North Pacific and the connection to the Arctic is too shallow, the deep branch of the overturning cell in the Pacific Ocean is supplied only from the south (Mantyla and Reid 1983).

Several studies suggest that the deep branch of the Pacific meridional overturning circulation (PMOC) is changing both in strength and temperature. In recent

Corresponding author address: G. Voet, Scripps Institution of Oceanography, University of California, San Diego, 8851 Shellback Way, La Jolla, CA 92093.
E-mail: gvoet@ucsd.edu

DOI: 10.1175/JPO-D-16-0063.1

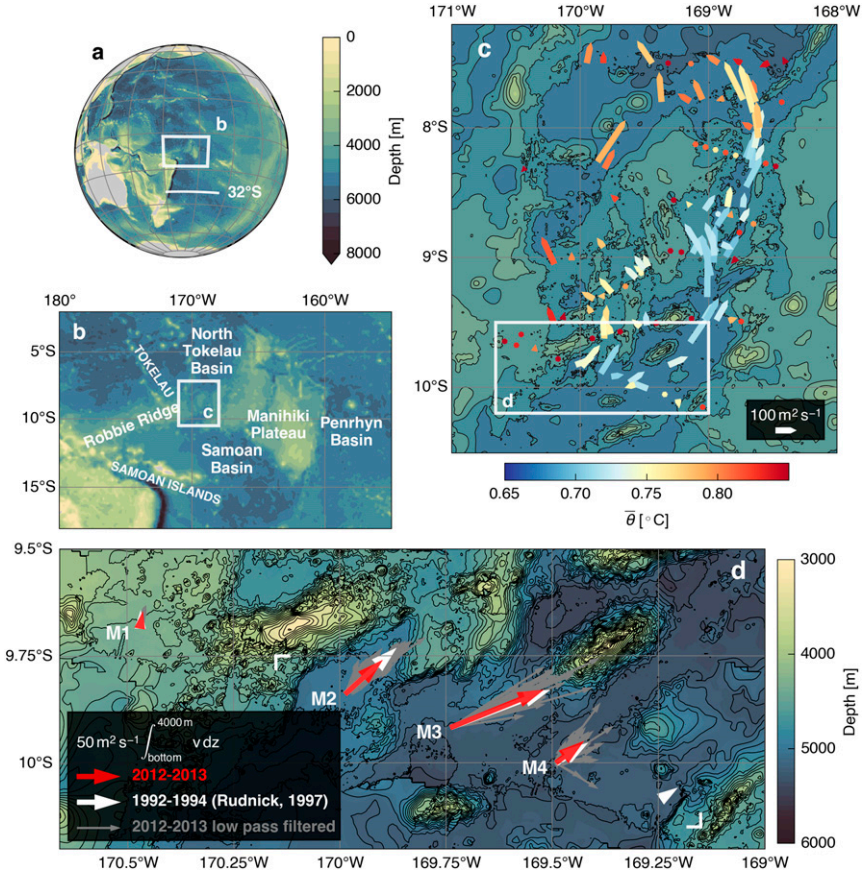

FIG. 1. (a) Bathymetry of the Pacific Ocean with the Samoan Passage at the center. The line at 32°S marks upstream measurements used in Sloyan et al. (2013). (b) Bathymetry of the Samoan Passage and surrounding bathymetric features. (c) Depth-integrated LADCP velocities below 1°C from shipboard observations in the Samoan Passage in 2012 (Voet et al. 2015); colors indicate velocity-weighted mean temperature of the abyssal layer below 1°C. Scale given to the lower right. (d) Depth-integrated time-mean velocities from moored time series below 4000 m. White arrows show the 1990s data, and red arrows show the 2010s data. Gray arrows show 100-h, low-pass-filtered snapshots of the 2010 depth-integrated velocity time series spaced by 200 h. All arrows are to scale given on the lower left. White corners depict zoom area of map in Fig. 7. Bathymetry shown is a combination of multibeam soundings and Smith and Sandwell global bathymetry (Becker et al. 2009).

decades the deep waters in the Pacific are warming (Fukasawa et al. 2004; Johnson et al. 2007; Purkey and Johnson 2010) and the abyssal layer of Antarctic Bottom Water (AABW) is contracting, associated with a slowdown in the bottom limb of the MOC (Purkey and Johnson 2012). A reanalysis study also suggests that the volume transport of the deep PMOC has been decreasing over the past decades (Kouketsu et al. 2011).

The Samoan Passage is the major gateway for the flow of dense bottom waters into the North Pacific (Reid and Lonsdale 1974). From hydrographic observations, Roemmich et al. (1996) estimated that 6.7 Sv, more than half of the 11.7 Sv northward volume transport at depth across 9°S, make their way through the Samoan Passage (Fig. 1). Minor northward flow was also observed west of the Samoan Passage across Robbie Ridge (1.1 Sv) and to the east around the Manihiki Plateau (2.8 Sv; Roemmich et al. 1996).

Moored measurements from the early 1990s (Rudnick 1997) carried out as part of the World Ocean Circulation Experiment (WOCE) provide the only previous time series of the abyssal volume transport through the Samoan Passage. The 17-month-long record had a time-mean volume transport of 6 Sv below 4000 m depth, with considerable variability on time scales from semidiurnal to annual.

We report here on a mooring array with updated deep measurements of the volume transport through the Samoan Passage. In the following, we present the results

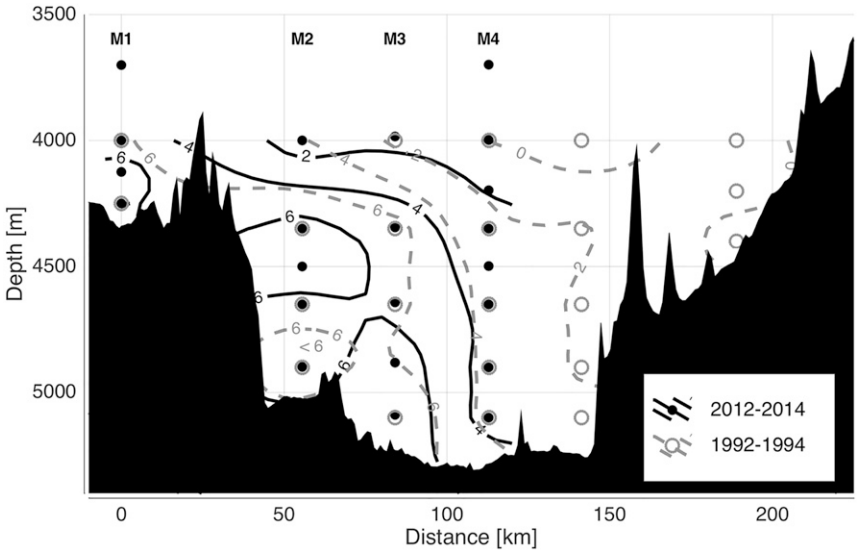

FIG. 2. Time-mean along-passage current (cm s^{-1}) for the 1990s (gray dashed contours) and 2010s velocity time series (black contours). Time-mean velocity fields were calculated from objectively mapped velocity time series for each period. Black dots show locations of RCM8 current meters on the 2010s moorings, and open circles show 1990s current meter locations. An overview of the mooring setup is given in Table 1.

from the mooring array with an overview of the measurements in section 2, volume transport calculations and a comparison to the 1990s volume transport and temperature in section 3, and a discussion of the results in section 4.

2. Data and methods

a. Mooring array

An array of four moorings was put in place at the entrance to the Samoan Passage from July 2012 to February 2014 (Fig. 1). The moorings were deployed during the first major cruise of the Samoan Passage Abyssal Mixing Experiment (SPAMEX) on board the R/V *Revelle* in July and August 2012. Results of this cruise are reported in Alford et al. (2013) and Voet et al. (2015). All moorings were successfully recovered during the second major SPAMEX cruise on board the R/V *Thompson* in January and February 2014. The four moorings were placed at the same locations as the western moorings in the six-element array from the early 1990s (Rudnick 1997). The volume transport in the eastern part of the passage was too small to justify the added expense of redeploying the two eastern moorings. The time-mean volume transport east of mooring M4 in the 1990s array was only 0.8 Sv, or less than 15% of the total volume transport (see section 3).

The moorings were equipped with Aanderaa Recording Current Meters (RCM8s) and acoustic Doppler current profilers (ADCPs) at various depths that coincided in most cases with depths of the instruments in the 1990s array (Fig. 2). An overview of the instruments on each of the moorings, labeled M1–M4, is given in Table 1. Most of the RCM8 current meters returned good data, with 90% of the instruments measuring for more than 1 year and more than 75% of the instruments lasting for the whole 18-month deployment period. Shorter time series were due to battery failure before mooring recovery. A total of 21 velocity time series were obtained, of which 15 come from the exact same location and depth as velocity time series in the 1990s array (Fig. 2). Two of the velocity time series on mooring M3 stem from single-point acoustic current meters (Teledyne RD Instruments Doppler volume sampler). The higher-resolution time series from these two instruments were averaged and downsampled to match the 1-hourly vector-averaging sampling procedure of the RCM8s. All moorings were designed to withstand strong current conditions in the abyssal flow. Pressure records from moorings M2–M4 indicate that the moorings stood upright in the water, and intended instrument depths were matched to within the uncertainty of the pressure measurements. The pressure recorder at mooring M1 flooded during deployment, and no depth information exists for this mooring. Given the stability in the vertical of the other three moorings with standard deviations in pressure of less than 1 dbar, and precision in placing these at the correct positions, we assume that M1 also stood upright and at the correct bottom depth. In

TABLE 1. Location, configuration, and data return of the moorings. Variables denote velocity amplitude and direction (**V**) and temperature (T).

Mooring ID	Position and depth	Depth (m)	Duration (days)	Type	Variables
M1	170°28.218′W,	3700	562	RCM8	**V**, T
	9°41.112′S;	4000	519	RCM8	**V**, T
	4336	4124	562	RCM8	**V**, T
		4250	545	RCM8	**V**, T
		4251	568	SBE39	T
		4321	568	SBE39	T
M2	169°59.256′W,	3999	562	RCM8	**V**, T
	9°50.382′S;	4349	542	RCM8	**V**, T
	5017	4500	559	RCM8	**V**, T
		4650	562	RCM8	**V**, T
		4899	524	RCM8	**V**, T
		4900	567	SBE39	T
		5001	567	SBE39	T
M3	169°44.400′W,	3984	555	RCM8	**V**, T
	9°55.092′S;	4344	381	RCM8	**V**, T
	5229	4643	555	RCM8	**V**, T
		4882	320	DVI	**V**
		5088	449	DVI	**V**, T
		5217	532	SBE39	T
M4	169°9.473′W,	3698	562	RCM8	T
	10°0.044′S;	3998	527	RCM8	**V**, T
	5288	4198	434	RCM8	**V**, T
		4349	518	RCM8	**V**, T
		4499	562	RCM8	**V**, T
		4650	562	RCM8	**V**, T
		4900	562	RCM8	**V**, T
		5100	556	RCM8	**V**, T
		5101	565	SBE39	T
		5270	565	SBE39	T

addition to the RCM8s, two ADCPs were attached to the upper part of mooring M3. The data return from the ADCPs was very poor because of the low-scattering environment at these great depths, and we therefore do not present the measurements here. Temperature was measured at all RCM8s (with the Arctic range setting) and at several Sea-Bird Electronics SBE 39 thermistors attached to the releases of the moorings (see Table 1 for instrument locations and depths). The temperature measurements from the RCM8s have a nominal accuracy of only $\pm 5 \times 10^{-2}$ °C and a resolution of $\pm 8 \times 10^{-3}$ °C. A comparison with nearby conductivity–temperature–depth (CTD) data (appendix A) shows that accuracies for our measurements and the 1990s data are slightly better than nominally specified, at $\pm 3 \times 10^{-2}$ °C. SBE 39 thermistors measured at accuracy and resolution of $\pm 2 \times 10^{-3}$ °C and $\pm 1 \times 10^{-4}$ °C, respectively.

b. *Hydrographic data*

Shipboard hydrographic measurements across the Samoan Passage were carried out during the deployment and recovery cruises in 2012 and 2014 with a Sea-Bird SBE 911plus CTD attached to a water sample rosette. In addition, historical hydrographic measurements collected in the Samoan Passage as part of WOCE and Climate and Ocean: Variability, Predictability and Change (CLIVAR) were downloaded from the Global Ocean Ship-Based Hydrographic Investigations Program (GO-SHIP; http://www.go-ship.org) data repository. Table 2 shows an overview of the hydrographic profiles available in the vicinity of the mooring array.

c. *Objective mapping*

Velocity vector and temperature fields are objectively mapped following Roemmich (1983). First, a large-scale planar field is fitted in a least squares sense to the data. The large-scale field is then subtracted from the observations and the residuals are fitted again. This time the fitting is based on an exponential function that models the expected products between estimated field and measured values based on spatial decorrelation scales and the allowed deviation between observation and fit.

TABLE 2. Hydrographic data along the mooring array across the Samoan Passage with number of stations and principal investigator (PI).

Year	Number of stations	PI
1992	11	Rudnick
1994	14	Roemmich
1996	7	Bullister
2001	6	Wijffels
2009	6	Sloyan
2012	12	Alford
2014	5	Alford

The decorrelation scales for the small-scale field were chosen to be 30 km in the horizontal and 300 m in the vertical to be roughly equivalent with instrument spacing. Deviations between observation and fit are minimized. The objectively mapped field is finally the sum of modeled large- and small-scale fields. Integral quantities in this study, like volume transport, are then simple summations over the objectively mapped fields. Objective mapping techniques and parameters used here are in accordance with Rudnick (1997).

3. Results

The overall structure of the abyssal current in the Samoan Passage is remarkably similar compared to conditions in the early 1990s. The time-mean direction of the depth-integrated current in 2012–14 matches the time-mean, depth-integrated current directions from the 1990s data to within 8° (Fig. 1). The amplitude of the time-mean, depth-integrated currents was reduced by 27% and 12% compared to the earlier measurements at moorings M2 and M3. Depth-integrated, time-mean currents at M1 and M4 show have the same amplitudes as their 1990s counterparts.

In the vertical, the time-mean flow is split into two cores with velocities above 6 cm s^{-1} (Fig. 2). This is the same structure as for the 1990s data with slightly reduced amplitudes of the two cores when averaged over time. The velocity structure at mooring M4 is almost identical to its 1990s counterpart.

Following Rudnick (1997), the volume transport is calculated as the spatial integral over the objectively mapped velocity fields between the moorings below 4000 m depth (Fig. 3). Volume transport east of mooring M4 is scaled from the volume transport west of M4 (appendix B).

The reduction in time-mean current amplitudes presented above is reflected by a reduced time-mean volume transport for the 2012–14 period when compared to the 1990s. Our best estimate for the total time-mean volume transport through the Samoan Passage from July 2012 to October 2013 is 5.4 Sv. This estimate consists of 4.7 Sv through the western part of the passage between moorings M1 and M4 and 0.7 Sv through the eastern part east of mooring M4. The overall volume transport through the Samoan Passage was reduced by 0.5 Sv compared to the early 1990s. The uncertainty of

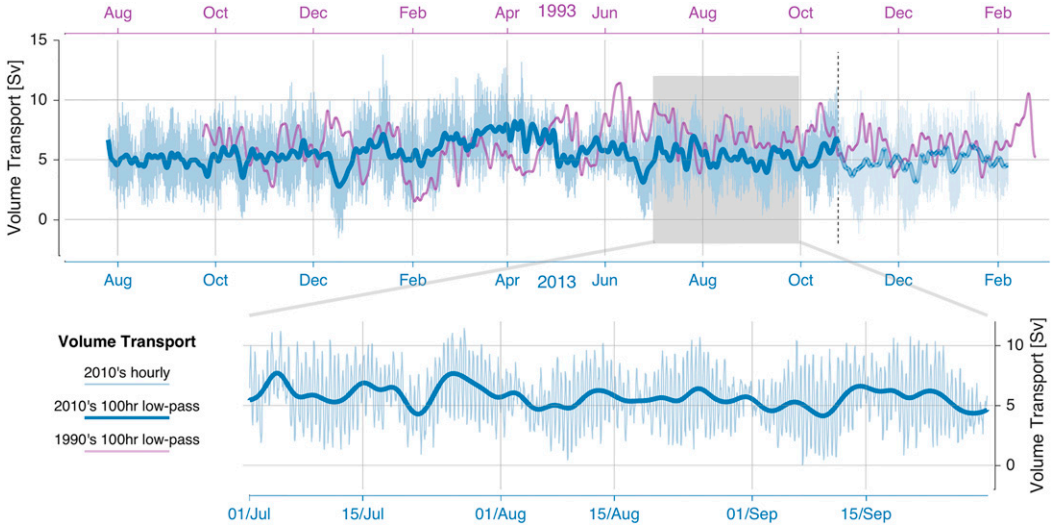

FIG. 3. Volume transport below 4000 m depth from objectively mapped velocity time series. (top) The time series over the whole deployment period; (bottom) a zoom-in of the 3-month period from July to September 2013. Light blue lines show hourly volume transports, and dark blue lines show the 100-h, low-pass-filtered volume transport time series. The uncertainty of the volume transport estimate increases significantly after October 2013, when several instruments stopped working, as indicated by lighter colors and the dashed line in the top panel. The low-pass-filtered version of the recalculated 1990s volume transport time series is shown in purple.

our volume transport estimate, due to the horizontal spacing of the moorings, the vertical spacing of the instruments, the limited length of the time series, and missing data from the eastern part of the passage is ±0.6 Sv at 95% confidence limits and ±0.4 Sv at 68% confidence limits (appendix B).

About half of the volume transport carries water with potential temperatures less than 0.7°C (Table 3). The volume transport reduction in comparison to the 1990s is evenly spread over temperature classes with a reduction of 0.3 Sv in the coldest class below 0.7°C and increasing to 0.6 Sv for all water colder than 0.95°C, corresponding almost exactly to the results for volume transport below 4000 m discussed above. Note that uncertainties in volume transport would become significantly larger above 4000 m because of limited instrument coverage (Fig. 2).

The volume transport through the Samoan Passage is highly variable. Tidal velocity variations modulate the volume transport at semidiurnal frequencies. A fortnightly modulation of the tidal signal is striking (Fig. 3, zoom), but does not seem to affect the low-pass-filtered volume transport. Rudnick (1997) found increased volume transport variability in a band around the 30-day period. This variability is apparent for the 1990s dataset in spectra from volume transport time series for all temperature classes (Fig. 4). In contrast, variability in the 30-day period band is barely visible in frequency spectra of the recent volume transport time series. A wavelet analysis of the 1990s volume transport time series shows that the 30-day period variability is not a persistent feature throughout the time series, but rather occurred sporadically with intense periods in February and June 1993 (Fig. 5). The recent measurements also show increased energy levels in this spectral band, but only for a shorter period around January 2013. Hence, the overall peak is reduced in Fig. 4. Peaks at the near-inertial frequency are apparent in the volume transport spectra from both observational periods, with decreasing

TABLE 3. Time-mean volume transport in temperature classes. West denotes the volume transport between moorings M1 and M4, and 1990s full shows the volume transport between moorings R1 and R6 from the 1990s array.

θ (°C)	2010s west (Sv)	1990s west (Sv)	1990s full (Sv)
<0.95	4.7	5.2	6.0
<0.90	4.4	4.8	5.6
<0.85	4.1	4.5	5.2
<0.80	3.7	4.0	4.7
<0.75	3.2	3.5	4.1
<0.70	2.4	2.7	3.2

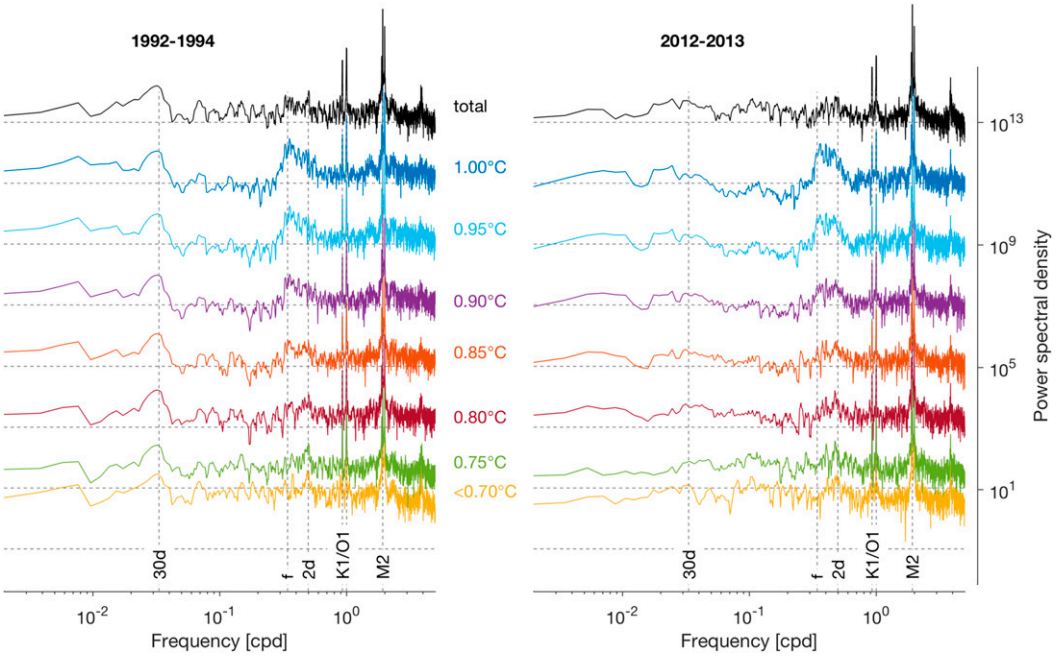

FIG. 4. Power spectral density estimates of volume transport time series (total and in temperature classes). (left) Spectral estimates for the 1990s data and (right) for the recent volume transport time series. The 30-day (30d), near-inertial (f), 2-day (2d), diurnal (K_1, O_1), and semidiurnal M_2 periods are marked with vertical lines. Power spectral density estimates for the 1990s dataset are calculated from the R4 volume transport time series, that is, excluding the volume transport in the eastern part of the passage. Spectral estimates are plotted in a variance-preserving manner and offset by two octaves between each temperature class for plotting clarity.

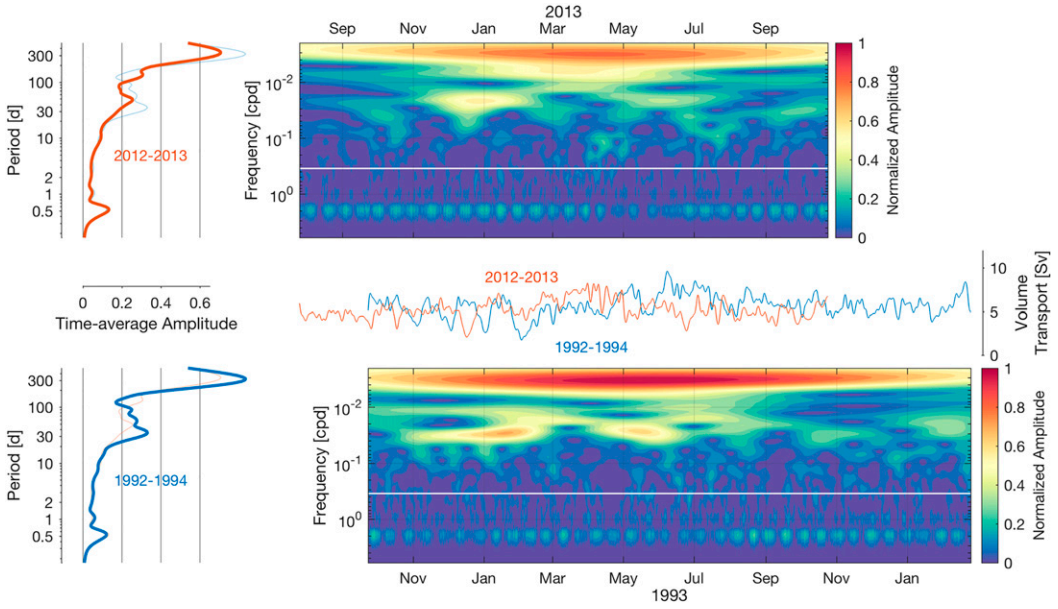

FIG. 5. Wavelet-derived spectrogram of the volume transport time series. Shown are the (left) the time-mean amplitudes of the spectrogram for (top) recent data and (bottom) the Rudnick data; (right) panels are lined up to match the seasonal scale. The white line shows the inertial period of about 3 days. The center panel shows both the 1990s and 2010 volume transport time series plotted on the same seasonal scale.

energy toward colder temperature classes (Fig. 4). Rudnick (1997) ascribed this to proximity of bottom topography inhibiting the lateral scales of near-inertial waves. Alternately, the waves may lose energy as they propagate downward. The near-inertial peak starts to diminish at warmer temperature classes for the recent data, and this may be due to isotherms being located at greater depths (and thus likely laterally closer to topography) than in the previous measurements, as we will show below. The spectrogram in Fig. 5 shows that variability in the near-inertial band occurs sporadically, as expected for near-inertial waves forced by storms. It is interesting to note that spectral peaks at a period of about 2 days in the colder temperature classes clearly occur at the same times as near-inertial variability, hinting to near-inertial waves being forced into higher frequencies as they approach the deeper layers.

Various measurements indicate a significant warming of the abyssal flow through the Samoan Passage. Hydrographic observations over the past two decades show how isotherms successively deepened over the years, with the recent occupations showing isotherms at their deepest locations in the whole dataset (Fig. 6a). While internal tides and near-inertial waves lead to significant isotherm depth variability at the entrance to the Samoan Passage with peak-to-peak amplitudes of up to 100 m (Voet et al. 2015), a month-long time series from a McLane Moored Profiler (MP) deployed at the M3 location in July and August 2012 indicates that the isotherm deepening exceeds the short-term variability. The MP measured temperature with an SBE 52 CTD at a nominal accuracy of ± 0.002°C [for further details on the MP deployment, see Voet et al. (2015)]. The MP observations show that the isotherm depth ranges given by plus/minus two standard deviations around their time-mean isotherm depth are deeper than isotherms observed in the early 1990s. Potential temperature profiles from the deep part of the section from 1992 and 2012 are clearly separated by 0.015°C (Fig. 6b). We quantify the isotherm descent over time by applying linear fits to the isotherm slopes between 50 and 150 km for each section occupation. Evaluation of the fits at 100 km and a second linear fit to these isotherm depths over time shows descent rates of about 30 m decade^{-1} in the layers above 0.7°C and descent rates of more than 100 m decade^{-1} in the coldest waters (Fig. 6c). The descent rate of the coldest isotherm shown here (0.67°C) increased sharply in recent years while the descent rates of warmer isotherms above show a more linear trend.

A closer look at temperatures in bottom proximity in the deeper parts of the section reveals that indeed the warming here did not start before the mid-2000s, with potential temperatures around 0.65°C near the bottom from 1992 through 2001 (Fig. 7). The 2009, 2012, and 2014 near-bottom observations show a trend toward 0.67°C over the past decade. Again, moored time series indicate this warming being significant above short-term variability. Data from three thermistors attached to the

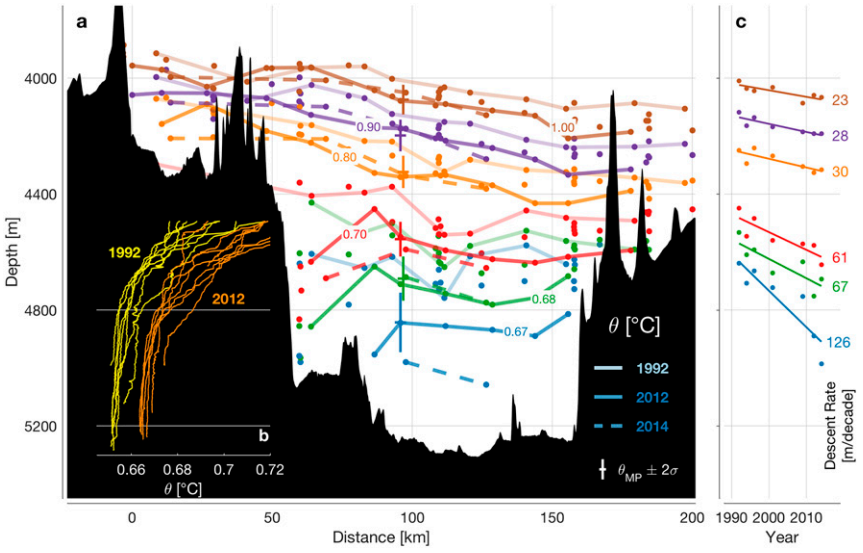

FIG. 6. (a) Isothermal depths from hydrographic observations along the mooring array. Data from all cruises in Table 2 are shown with dots. Data from 1992, 2012, and 2014 are also contoured. Moored profiler observations from August 2012 (Voet et al. 2015) are shown with their mean isotherm depth plus/minus two standard deviations. (b) Profiles of potential temperature from 1992 (yellow) and 2012 (orange) from the deep part of the section plotted on the same depth axis as the main plot. (c) Isotherm depths at 100 km from linear fits to all profiles per hydrographic dataset (dots) and linear trends to isotherm depths at 100 km showing isotherm descent rates over the period 1992–2014 (lines). Numbers show isotherm descent rates per decade. Isotherm colors match those in main panel. Depth axis as in (a).

releases on moorings M2–M4 show that all 2012 and 2014 observations fall within ±2 standard deviations of the time mean over the deployment period of the mooring array. Bottom temperatures from the 1990s are outside the range of the thermistors.

Moored temperature time series from the RCM8s indicate that the time-mean temperature of the flow is about 0.02°C higher than 20 years ago (Fig. 8). At most locations where RCM8s were placed at the same depths as at the 1990s array, the time-mean temperature differences vary between about 0.015°C in the colder layers and about 0.025°C in the warmer layers. Only the instrument at 4000 m at mooring M4 differs from this scheme, and it could not be verified if this was due to a calibration issue. The warming observed with the RCM8 temperature sensors is within their accuracy of 3×10^{-2}°C (appendix A) and thus statistically not different from zero. However, the warming trend found here is consistent with CTD and thermistor measurements above.

Temperature measurements were objectively mapped to calculate section-averaged time series. The section-averaged temperature time series below 4000 m (Fig. 9) shows interseasonal variability in both the 1990s and the 2010s data. The 2012/13 time-mean of the section-averaged temperature is about 0.02°C warmer than in the 1990s, reflecting the warming trend seen in Fig. 8. However, the velocity-weighted, section-averaged temperature calculated by weighing with objectively mapped velocities normal to the section did not change compared to the 1990s.

4. Discussion and conclusions

The moored time series presented here show that the overall volume transport of dense water below 4000 m through the Samoan Passage decreased by about 0.5 Sv or 8% compared to measurements two decades earlier. Because of uncertainties caused by the limited length of the time series, the spacing of the instruments within the mooring array, and missing measurements in the eastern part of the passage, this reduction is only statistically significant within 68% confidence limits (±0.4 Sv), but not within 95% confidence limits (±0.6 Sv, appendix B). We thus term the volume transport reduction compared to the 1990s likely, but not certain. Nevertheless, the reduction in volume transport found here agrees with several studies suggesting a slowdown of the PMOC in recent decades. In a reanalysis study, Kouketsu et al. (2011) find a slowdown of the deep PMOC between 0.5 and 1 Sv decade^{-1}. Decadal hydrographic surveys upstream of the Samoan Passage analyzed by Sloyan et al. (2013) show a 1.7-Sv decrease in geostrophic northward

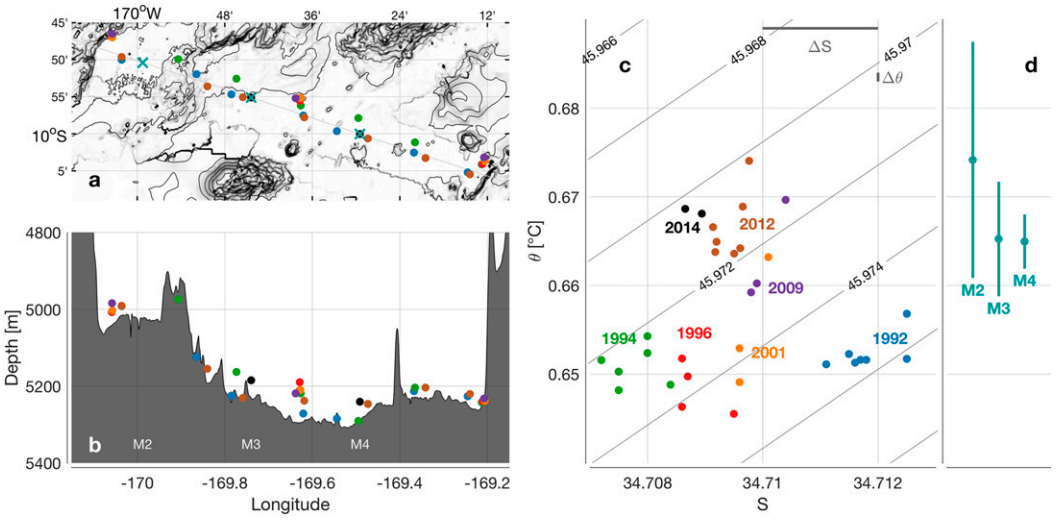

FIG. 7. Near-bottom temperatures in hydrographic datasets and moored thermistors. (a) Locations of hydrographic profiles (dots) and moorings M2–M4 (crosses). Zoom area depicted in Fig. 1d. (b) Depth of deepest observation in hydrographic profiles. (c) The θ–S diagram of the deepest observation in hydrographic profiles from different years. Uncertainties in salinity ($\Delta S = 0.002$) and temperature ($\Delta\theta = 0.001$°C) are shown to the upper right. (d) Time-mean plus/minus two standard deviations of temperature time series from three thermistors (SBE 39) attached to moorings M2, M3, and M4, respectively. Moored time series were recorded for the whole deployment period from 2012 through 2014.

volume transport across 32°S (Fig. 1) over the period 1996–2009 because of a decreasing density gradient across the southwest Pacific basin. From global hydrographic observations over the 1990s and 2000s, Purkey and Johnson (2012) infer a reduction in abyssal northward volume transport into the North Pacific of about 2 Sv from a volume balance and 0.65 Sv from heat budgets.

The abyssal flow through the Samoan Passage warmed significantly over the past two decades at a rate of approximately 1×10^{-2} °C decade^{-1}. The observed warming agrees with studies showing a general warming of

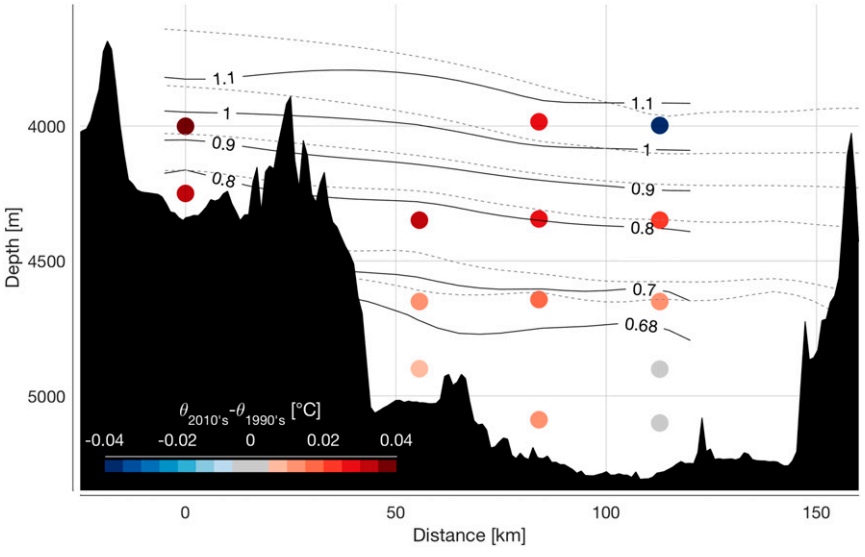

FIG. 8. Time-mean temperature difference at RCM8 temperature sensors that are collocated in depth and position with instruments from the 1990s array (colored dots). Time-mean temperature field from objectively mapped temperature time series from the 1990s (gray dashed) and the 2010 data (black).

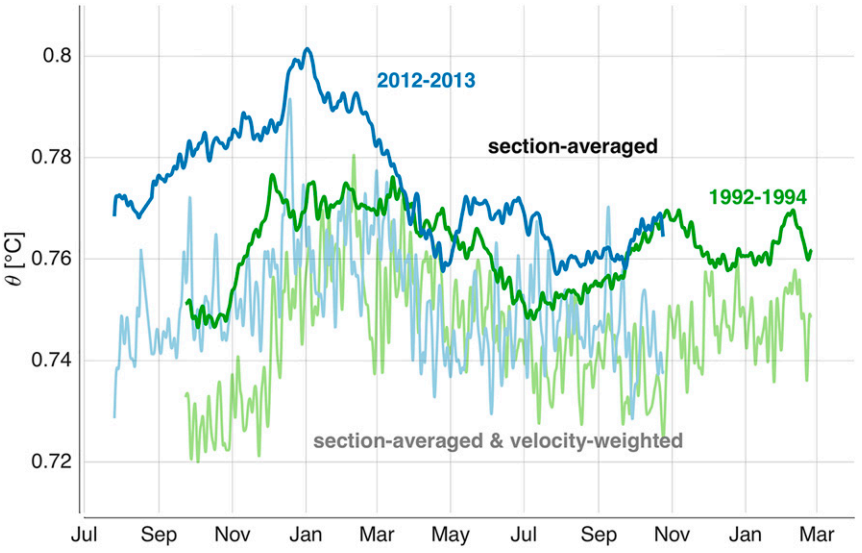

FIG. 9. Time series of section-averaged RCM8 temperature (darker colors) and velocity-weighted, section-averaged RCM8 temperature (lighter colors) for the 1990s (green) and the 2010s (blue) deployment periods. Both time series are plotted on the same seasonal axis.

AABW in the world's oceans (Purkey and Johnson 2010). From basin heat budgets, Purkey and Johnson (2012) infer a warming of 0.013°C for AABW in the Samoan Passage over a time span of about 20 years. Warming of AABW at a rate of 2–3 $\times 10^{-2}$ °C decade^{-1} was observed in the Vema Channel in the South Atlantic (Zenk and Morozov 2007). Upstream of the Samoan Passage, Sloyan et al. (2013) find a warming trend of 1.4×10^{-2} °C decade^{-1} in repeat occupations of WOCE standard section P15 along the western boundary of the southwestern Pacific. Earlier signals of abyssal warming in the North Pacific (Kawano et al. 2006) were probably communicated via planetary boundary waves (Masuda et al. 2010). Repeat chlorofluorocarbon (CFC) measurements in the Samoan Passage and in the deep western boundary current upstream suggest that the warming observed here is an advected signal from the source regions in the Southern Ocean (J. Bullister 2016, personal communication). CFCs have a unique history of concentration in the atmosphere, with a sharp increase due to strong emissions between the 1960s and 1990s and a decline caused by international regulations thereafter, making them an excellent tracer in the ocean (Fine 2011). The temperature measurements in the near-bottom layer (Fig. 7) indicate that this advected signal of AABW warming arrived in the Samoan Passage after 2001, as observations from this year still fall in line with temperatures observed in the 1990s.

The warming of the abyssal flow corresponds to a general deepening of isotherms (and isopycnals) in our observations. Again, this is in agreement with upstream observations as Sloyan et al. (2013) find isopycnal sinking at a rate of about 100 m decade^{-1} for neutral density $\gamma^n = 28.2$ kg m^{-3} in the AABW layers. Neutral density is a continuous analog of potential density surfaces discretely referenced to certain depths (Jackett and McDougall 1997). However, they do not observe isopycnal sinking for $\gamma^n = 28.1$ kg m^{-3}. In the Samoan Passage, isotherms below $\theta = 0.7$°C, corresponding to γ^n in the range 28.18–28.20 kg m^{-3} (Voet et al. 2015, Fig. 3), sank between 60 and 100 m decade^{-1}, whereas in the warmer layers above, the sinking rates were less than 30 m decade^{-1}. The sinking of isopycnals may indicate a larger reduction in the overall flow of abyssal waters into the North Pacific than observed here for the Samoan Passage. If the deepening of isopycnals occurs over Robbie Ridge or along the Manihiki Plateau (Fig. 1), a reduction of the abyssal geostrophic northward flow in these areas is expected. This reduction may be most pronounced in the flow across the relatively shallow Robbie Ridge. A significant reduction of the small abyssal volume transport of $O(1)$ Sv across Robbie Ridge could contribute as much to a general slowdown of the PMOC as the reduction in the Samoan Passage indicated by our measurements.

Warming of the flow through Samoan Passage implies excess heat transport and a heat content increase in the abyssal North Pacific. Purkey and Johnson (2010) find a heat content change for the North Pacific below 4000 m depth corresponding to an equivalent heat flux of 3×10^{-2} W m^{-2}. Consistently, at a volume transport of 6.0 Sv, the warming of 2×10^{-2} °C in the Samoan Passage

corresponds to an excess heat flux of about 5×10^{11} W or an equivalent heat flux of about 1×10^{-2} W m^{-2} for the North Pacific. The excess heat flux due to warming in the Samoan Passage integrated over the past 20 years results in a heat content change of 3×10^{20} J for the Pacific north of the Samoan Passage. This is a small change compared to an estimated industrial era heat content change of 5×10^{22} J for the global deep oceans below 2000 m so far (Purkey and Johnson 2010; Gleckler et al. 2016). It reflects the remoteness of the abyssal North Pacific from its ventilation sources and its dependence on the flow through the Samoan Passage for renewal of bottom waters.

Weakening flow counteracts the excess heat transport due to warming in the Samoan Passage. A reduction in volume transport at the current warming rate may be expected to scale approximately linearly, that is, a 10% flow reduction implies 10% reduction in (excess) heat transport into the abyssal North Pacific. This holds especially true with the volume transport reduction occurring across all temperature classes (Table 3). The data shown in Fig. 9 provide a qualitative estimate of the relative importance of warming and weakening flow in the Samoan Passage: the section-averaged, time-mean temperature increased by about 2×10^{-2} °C while the velocity-weighted, section-averaged, time-mean temperature stayed virtually constant.

Recent studies show increasing heat uptake of the global deep oceans (Gleckler et al. 2016), thereby tempering Earth's surface warming associated with the greenhouse effect. The warming of the abyssal flow through Samoan Passage presented in this study supports these findings, as it suggests excess heat transports into the North Pacific. However, if the slowdown of the PMOC indicated by our results continues, these excess heat transports may weaken, thereby limiting the potential for future heat uptake of the abyssal North Pacific.

Acknowledgments. We thank Eric Boget for his exemplary assistance in designing, deploying, and recovering the moorings; Keith Magness, Trina Litchendorf, Andrew Cookson, Zoë Parsons, Andy Pickering, Kelly Pearson, Janna Köhler, Tessa Tafua, Deepika Goundar, Samuel Fletcher, Tahmeena Aslam, Thomas Decloedt, Alofa Aleta, and Vaatele Tauinaola for their assistance in making the measurements; and the captains and crews of the R/V *Revelle* and R/V *Thompson* for their skill in handling and operating the vessels, without which these measurements would not have been possible. Daniel Rudnick kindly provided previous mooring data. Sarah Purkey provided helpful comments on an earlier version of this manuscript. Two anonymous reviewers provided valuable comments that helped to improve this study. This work was funded by the National Science Foundation under Grants OCE-1029268 and OCE-1029483.

APPENDIX A

RCM8 Temperature Sensor Uncertainty

Temperature sensors on the Aanderaa RCM8s have a nominal accuracy of 5×10^{-2} °C. Comparison of RCM8 temperature measurements in the Samoan Passage with nearby CTD observations (90 data pairs in total) shows that 95% of all observations fall within a range of $\pm 3 \times 10^{-2}$ °C and 80% of all observations within a range of $\pm 2 \times 10^{-2}$ °C. Figure A1 shows temperature differences between RCM8 measurements and CTD observations close in time and space for both the 1990s and the 2010s dataset. Of the differences between RCM8 and CTD, 80% are less than $\pm 2 \times 10^{-2}$ °C, and a fit to the probability distribution of the differences results in a standard deviation $\sigma = 0.015$°C; thus, 95% of the RCM8 temperature measurements are expected to be within $\pm 3 \times 10^{-2}$ °C of the CTD observations. The differences shown here are conservative estimates of uncertainties in RCM8 temperature measurements as the CTD profiles used in the comparisons were up to 9 km away from the mooring sites and the time between concurrent observations was up to 45 days.

APPENDIX B

Volume Transport Calculation and Error Estimate

Volume transport was calculated following Rudnick (1997) as the spatial integral over objectively mapped velocity fields. For volume transport in temperature classes, objectively mapped temperature fields were also used. Applying this method to the 1990s data yields a time-mean volume transport of 6.0 Sv, thus reproducing the results from Rudnick (1997). Leaving out the two easternmost moorings yields a time-mean of 5.2 Sv in the recalculation of the 1990s volume transport. Volume transports in the east (between Rudnick moorings 5 and 6) and west are positively correlated with $r = 0.8$ at zero lag. Therefore, we account for the missing velocity measurements in the east in our dataset by linearly scaling the western transport to the east in the 1990s data where both transports are known. The constants m and c for the linear relationship

$$T_{\text{east}} = mT_{\text{west}} + c \tag{B1}$$

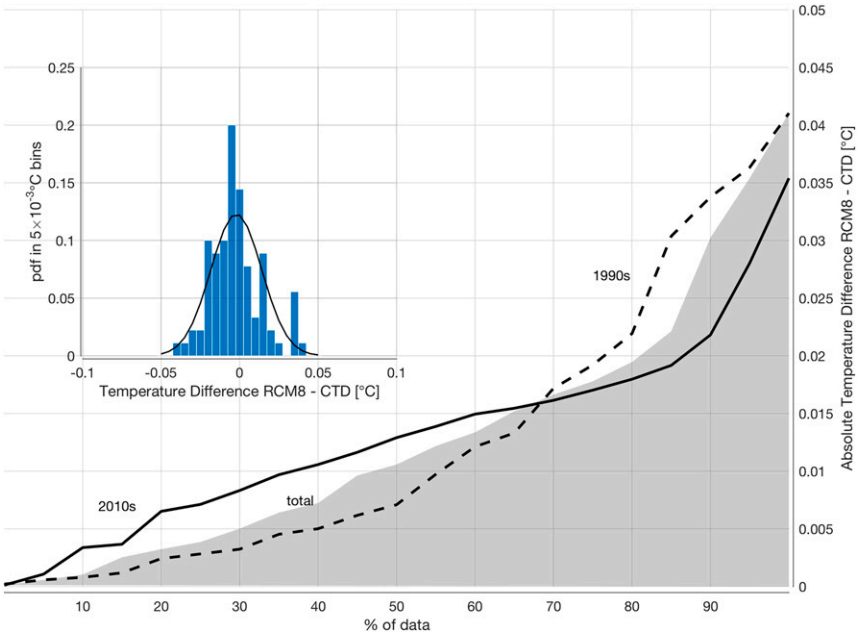

FIG. A1. Differences between moored RCM8 temperature measurements and CTD observations where close in time and space. The main plot shows the differences in percentiles for all data (gray), the 2010s deployments (black straight line), and the 1990s deployments (dashed black line). The total number of data pair differences shown here is 90. The inset shows a histogram of the temperature differences between RCM8 and CTD measurements with a normal fit to the probability distribution.

are determined with a least squares fit of the western to the eastern hourly volume transport estimates for the 1990s data (Fig. B1) to $c = -0.88$ and $m = 0.33$.

Errors in the time-mean volume transport estimates are due to the horizontal spacing of the moorings, the vertical spacing of the instruments, the limited length of the time series, and missing data from the eastern part of the passage. The spatial distribution of instruments at moorings M1–M4 is almost identical to the 1990s dataset, and we stick with the formal rms error of 0.3 Sv from Rudnick (1997) associated with mooring and instrument spacing. The expected error of the time-mean due to the limited length of the time series is estimated from its standard deviation σ as

$$\varepsilon = \frac{2\sigma}{\sqrt{N_{\mathrm{DOF}}}}, \tag{B2}$$

with the degrees of freedom N_{DOF} given by the length of the time series T divided by the decorrelation time scale t:

$$N_{\mathrm{DOF}} = T/(t-1). \tag{B3}$$

The normalized autocorrelation function of the 100-h, low-pass-filtered volume transport time series shows a significant drop below $1/e$ at a time scale $t = 16$ days; thus, the time series has 26 degrees of freedom at a total length of 446 days. With $\sigma = 1.0$ Sv, the expected uncertainty of the mean due to the limited length of the time series is 0.4 Sv. The uncertainty due to missing data from the eastern part is determined from the difference between simulated and measured eastern volume transports in the 1990s data. A fit to the normal distribution of these differences results in a standard

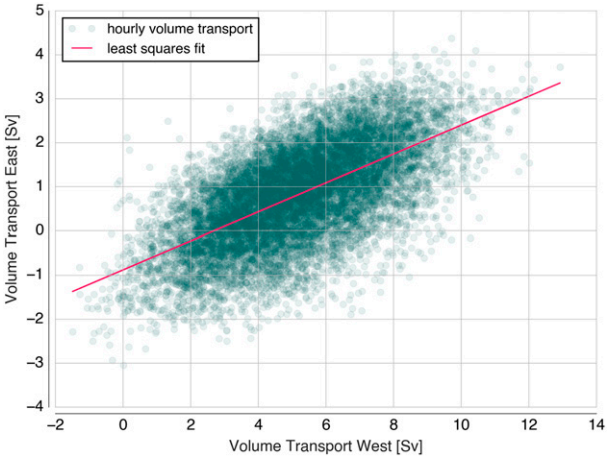

FIG. B1. Hourly volume transports in the 1990s data west of mooring M4 plotted against concurrent volume transports east of M4. The line shows a linear least squares fit to the data.

deviation of $\sigma_{PDF} = 0.85$ Sv. Calculating the uncertainty of the time mean of the simulated eastern transport as

$$\varepsilon_{east} = \frac{2\sigma_{PDF}}{\sqrt{N_{DOF}}} \quad \text{(B4)}$$

gives $\varepsilon_{east} = 0.3$ Sv. The overall uncertainty of our volume transport estimate is then calculated as the quadrature sum of the individual uncertainties, 0.6 Sv. Using 2σ in Eqs. (B2) and (B4) associates this uncertainty with the 95% confidence interval. The uncertainty within the 68% confidence interval is 0.4 Sv, calculated analogously using 1σ.

REFERENCES

Alford, M. H., J. B. Girton, G. Voet, G. S. Carter, J. B. Mickett, and J. M. Klymak, 2013: Turbulent mixing and hydraulic control of abyssal water in the Samoan Passage. *Geophys. Res. Lett.*, **40**, 4668–4674, doi:10.1002/grl.50684.

Becker, J., and Coauthors, 2009: Global bathymetry and elevation data at 30 arc seconds resolution: SRTM30_PLUS. *Mar. Geod.*, **32**, 355–371, doi:10.1080/01490410903297766.

Fine, R. A., 2011: Observations of CFCs and SF6 as ocean tracers. *Annu. Rev. Mar. Sci.*, **3**, 173–195, doi:10.1146/annurev.marine.010908.163933.

Fukasawa, M., H. Freeland, R. Perkin, T. Watanabe, H. Uchida, and A. Nishina, 2004: Bottom water warming in the North Pacific Ocean. *Nature*, **427**, 825–827, doi:10.1038/nature02337.

Gleckler, P. J., P. J. Durack, R. J. Stouffer, G. C. Johnson, and C. E. Forest, 2016: Industrial-era global ocean heat uptake doubles in recent decades. *Nat. Climate Change*, **6**, 394–398, doi:10.1038/nclimate2915.

Jackett, D. R., and T. J. McDougall, 1997: A neutral density variable for the world's oceans. *J. Phys. Oceanogr.*, **27**, 237–263, doi:10.1175/1520-0485(1997)027<0237:ANDVFT>2.0.CO;2.

Johnson, G., S. Mecking, B. Sloyan, and S. Wijffels, 2007: Recent bottom water warming in the Pacific Ocean. *J. Climate*, **20**, 5365–5375, doi:10.1175/2007JCLI1879.1.

Kawano, T., M. Fukasawa, S. Kouketsu, H. Uchida, T. Doi, I. Kaneko, M. Aoyama, and W. Schneider, 2006: Bottom water warming along the pathway of lower circumpolar deep water in the Pacific Ocean. *Geophys. Res. Lett.*, **33**, L23613, doi:10.1029/2006GL027933.

Kouketsu, S., and Coauthors, 2011: Deep ocean heat content changes estimated from observation and reanalysis product and their influence on sea level change. *J. Geophys. Res.*, **116**, C03012, doi:10.1029/2010JC006464.

Lumpkin, R., and K. Speer, 2007: Global ocean meridional overturning. *J. Phys. Oceanogr.*, **37**, 2550–2562, doi:10.1175/JPO3130.1.

Mantyla, A., and J. L. Reid, 1983: Abyssal characteristics of the World Ocean waters. *Deep-Sea Res.*, **30A**, 805–833, doi:10.1016/0198-0149(83)90002-X.

Masuda, S., and Coauthors, 2010: Simulated rapid warming of abyssal North Pacific waters. *Science*, **329**, 319–322, doi:10.1126/science.1188703.

Purkey, S. G., and G. C. Johnson, 2010: Warming of global abyssal and deep Southern Ocean waters between the 1990s and 2000s: Contributions to global heat and sea level rise budgets. *J. Climate*, **23**, 6336–6351, doi:10.1175/2010JCLI3682.1.

——, and ——, 2012: Global contraction of Antarctic Bottom Water between the 1980s and 2000s. *J. Climate*, **25**, 5830–5844, doi:10.1175/JCLI-D-11-00612.1.

Reid, J., and P. Lonsdale, 1974: On the flow of water through the Samoan Passage. *J. Phys. Oceanogr.*, **4**, 58–73, doi:10.1175/1520-0485(1974)004<0058:OTFOWT>2.0.CO;2.

Roemmich, D., 1983: Optimal estimation of hydrographic station and derived fields. *J. Phys. Oceanogr.*, **13**, 1544–1549, doi:10.1175/1520-0485(1983)013<1544:OEOHSD>2.0.CO;2.

——, S. Hautala, and D. Rudnick, 1996: Northward abyssal transport through the Samoan Passage and adjacent regions. *J. Geophys. Res.*, **101**, 14 039–14 055, doi:10.1029/96JC00797.

Rudnick, D., 1997: Direct velocity measurements in the Samoan Passage. *J. Geophys. Res.*, **102**, 3293–3302, doi:10.1029/96JC03286.

Sloyan, B. M., S. E. Wijffels, B. Tilbrook, K. Katsumata, A. Murata, and A. M. Macdonald, 2013: Deep ocean changes near the western boundary of the South Pacific Ocean. *J. Phys. Oceanogr.*, **43**, 2132–2141, doi:10.1175/JPO-D-12-0182.1.

Voet, G., J. B. Girton, M. H. Alford, G. S. Carter, J. M. Klymak, and J. B. Mickett, 2015: Pathways, volume transport and mixing of abyssal water in the Samoan Passage. *J. Phys. Oceanogr.*, **45**, 562–588, doi:10.1175/JPO-D-14-0096.1.

Zenk, W., and E. Morozov, 2007: Decadal warming of the coldest Antarctic Bottom Water flow through the Vema Channel. *Geophys. Res. Lett.*, **34**, L14607, doi:10.1029/2007GL030340.